Supporting Information

Drastic Improvement of Air Stability in an n-type Doped Naphtalene-diimide Polymer by Thionation

Diego Nava[†§], Younghun Shin[‡], Matteo Massetti[†§], Xuechen Jiao[¥¤], Till Biskup[#], Madan S. Jagadeesh[§], Alberto Calloni[§], Lamberto Duò[§], Guglielmo Lanzani[†§], Christopher R. McNeill[¥], Michael Sommer[‡], Mario Caironi[†*]*

† Center for Nano Science and Technology @PoliMi, Istituto Italiano di Tecnologia, Via Pascoli 70/3, Milano 20133, Italy.

§ Politecnico di Milano, Dipartimento di Fisica, P.za L. da Vinci 32, Milano 20133, Italy

‡ Institut für Chemie, Technische Universität Chemnitz, Straße der Nationen 62, 09111 Chemnitz, Germany

¥ Department of Materials Science and Engineering, Monash University, Wellington Road, Clayton, VIC, 3800, Australia

¤ Australian Synchrotron, 800 Blackburn Road, Clayton, VIC, 3168, Australia

* Mario Caironi: mario.caironi@iit.it

* Michael Sommer: michael.sommer@chemie.tu-chemnitz.de

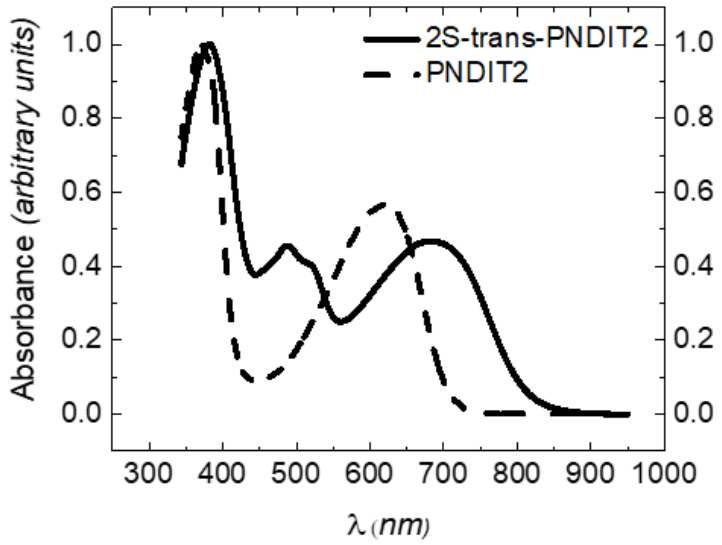

Figure S1. Uv-Vis-NIR absorption spectra of 2S-*trans*-PNDIT2 (solid line) and PNDIT2 (dashed line) in chloronaphthalene. [1]

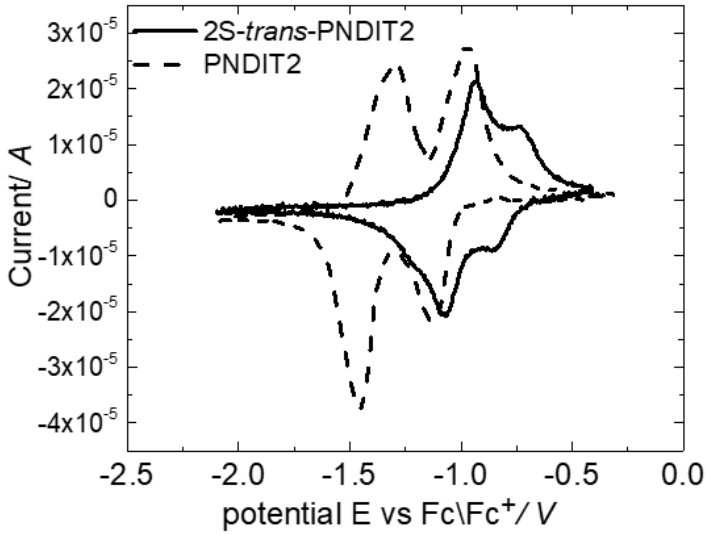

Figure S2. Cyclic voltammogram of thin films of 2S-*trans*-PNDIT2 (solid line) and PNDIT2 (dashed line). [1,2]

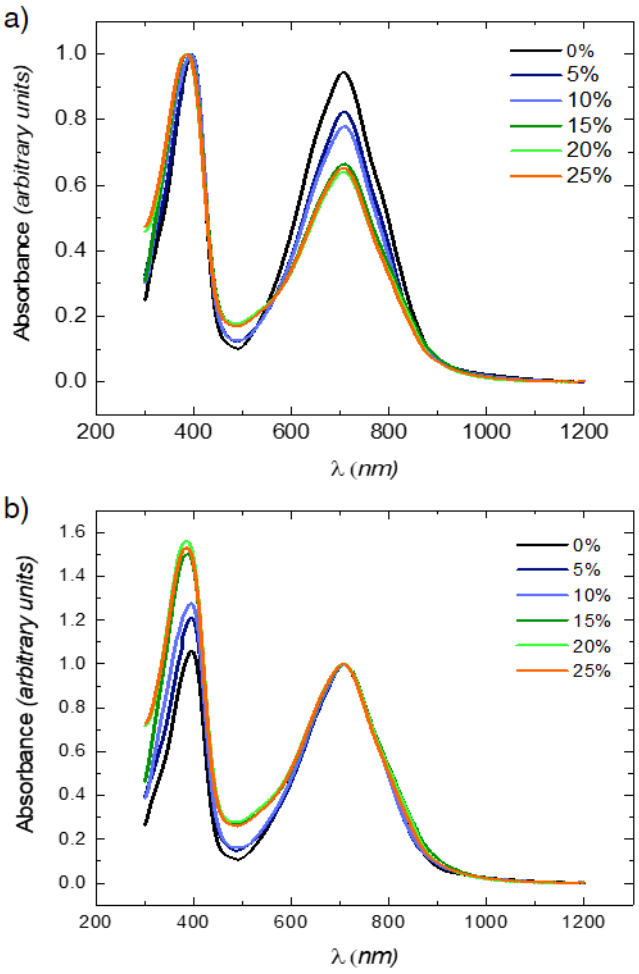

Figure S3. Uv-Vis-NIR thin film absorption spectra of PNDIT2 doped with different w/w concentration of N-DPBI. (a) Normalized at 386 nm and (b) at 709 nm.

Extraction procedure of HOMO and LUMO levels

The energy of LUMO level was extracted by the cyclic voltammetry plots reported in Figure S2. The reduction potential was determined by using the average of the reduction and corresponding oxidation, and the resulting value was referenced against ferrocene/ ferrocenium.

Given

$E_{LUMO} = ((E_{red} - E_{1/2(ferrocene)}) + 4.8)$ [3]

and

$E_{gap} = hc/\lambda_{on}$

with E_{gap} the optical bandgap, and λ_{on} the onset of the optical absorption as extracted by UV-Vis spectroscopy of chloronaphthalene solutions reported Figure S1.

Assuming that the optical bandgap of chloronaphthalene solutions is negligibly affected by aggregation features, the optical bandgap can be associated to the energy bandgap between HOMO and LUMO levels, so that:

$E_{HOMO} = E_{LUMO} + E_{gap}$.

X-ray photoemission spectroscopy (XPS) analysis

Photoemission measurements were performed by using an unmonochromatized Mg Kα lamp as the photon source ($h\nu$ = 1253.6 eV) and analyzing the photoemitted electron with a hemispherical spectrometer from SPECS GmbH operated at a pass energy of 20 eV (yielding an overall Full Width at Half Maximum resolution of 0.9 eV). These instruments are housed in the dedicated ultra-high vacuum system (10^{-8} Pa) described by Berti et al. [4]

The samples were prepared on Au covered glass slides following the procedure described in the experimental part and temporarily stored in a protective N_2 atmosphere. [5] The exposure to ambient conditions was limited to a few minutes before the insertion into the spectrometer. All the measurements were acquired at normal emission geometry, on freshly prepared samples kept at room temperature.

Figure S4 shows the detailed scans acquired on selected samples from the PNDIT2 (top) and 2S-*trans*-PNDIT2 (bottom) series, related to the N 1*s*, C 1*s* and S 2*p* binding energy (BE) regions. Filled symbols refer to undoped samples, while open symbols highlight the lineshape observed on samples loaded with 15% w/w of N-DPBI molecules. In order to compare the spectral lineshapes of all samples, we aligned the BE position of the main feature visible in the C 1*s* spectra (mainly related to photoemission from aromatic carbons in naphtalene/tiophene units and labeled C2 in Figure S4b), to the value of 285.0 eV.[6] Additionally, each spectrum was normalized to the photoemission intensity from the polymer (namely, to the S 2*p* spectral intensity) in order to highlight the contribution of N-DPBI molecules (containing only N and C atoms).

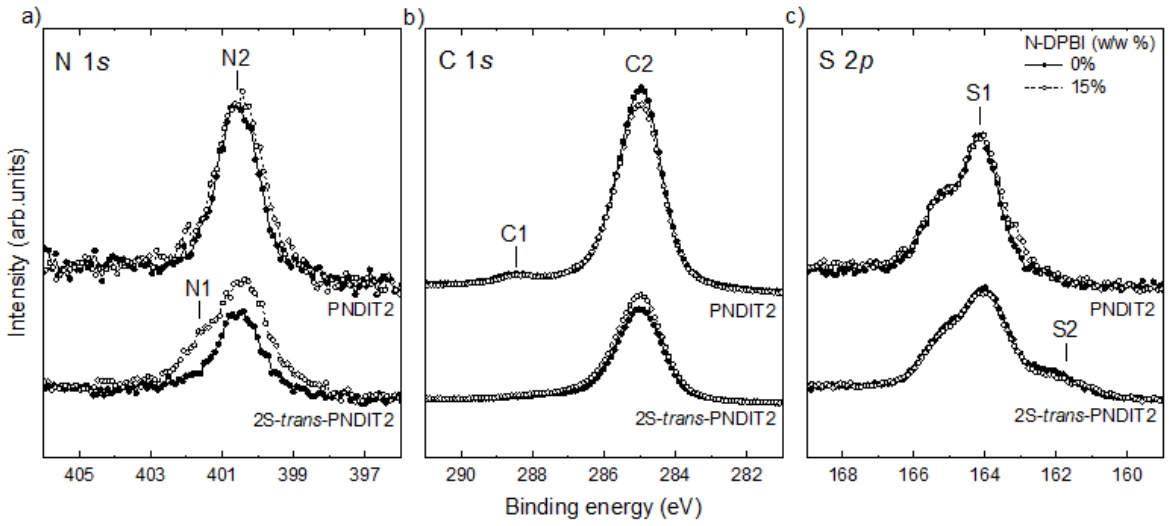

Figure S4. XPS results for (a) N 1*s* (b) C 1*s* and (c) S 2*p* regions, measured on representative samples from the PNDIT2 (top spectra) and 2S-*trans*-PNDIT2 (bottom spectra) series. Filled symbols refer to neat samples, while open ones to samples doped with 15 % w/w of N-DPBI molecules. Letters mark the most relevant features discussed in the text. All spectra are normalized to the intensity of the corresponding S 2*p* line. Source satellites have been always subtracted.

The N 1s spectra Figure S4a from the undoped samples show a single feature at a BE of about 400.5 eV (*i.e.* 115.5 eV from C2, in agreement with previous results on naphtalene[6] and perylene diimide[7,8]). No additional features are observed on doped PNDIT2 samples, while a shoulder at higher BE is detected on doped 2S-*trans*-PNDIT2 samples, expecially on those with a higher concentration of dopants. The shoulder (feature N1 in Figure S4a) can be reproduced (not shown) by adding to the main peak a symmetric (Voigt-like) lineshape centered at a BE of about 402 eV. Regarding the C 1*s* spectra (Figure S4b**)**, photoemission from PNDIT2 gives rise to feature C1, chemically shifted by about 2.5 eV from C2 and assigned to imide C,[9] together with shake-up satellites located at about 1.5-2.0 eV from the main lines.[10] In 2S-*trans*-PNDIT2, the partial substitution of O with S gives rise to chemically inequivalent imide C atoms resulting in a rather unresolved tail at the high BE side of C2. The S 2*p* spectra, Figure S4c, show, for the PNDIT2 series, a single doublet characteristic of photoemission from S atoms in thiophene groups (the S $2p_{3/2}$ peak, labeled S1 on panel c, is found at a BE of 164.0 eV, as also reported in Ref. (6)). The spectra acquired on 2S-*trans*-PNDIT2 samples show an additional doublet (label S2 marks the position of the S $2p_{3/2}$ peak), located at a smaller BE (by about 2 eV) than that of the main doublet and related to photoemission from thiones.[11,12]

Within the depth probed by our photoemission experiment (about three times the photoelectrons inelastic mean free path, here equal to 3±1 nm[13]) and notwithstanding the variability observed in the experimental data, we find that the addition of N-DPBI molecules results in clear changes in the spectroscopic lineshapes only for the 2S-*trans*-PNDIT2 series, with an increase in the intensity of feature N2 and the development of feature N1, Figure S4a. This is compatible with the detection of N-DPBI molecules. According to the available literature on the parent compound (4-(1,3-dimethyl-2,3-dihydro-1Hbenzoimidazol-2-yl)phenyl)dimethylamine (N-DMBI)[14] indeed, photoemission from N atoms in N-DPBI should give rise to a feature located at a BE of about

400 eV, *i.e.* almost overlapping with the signal from the polymers, while the shoulder can be related to the presence of oxidized N-DPBI molecules, generally considered as an indicator for the successful activation of dopant species.[14,15]

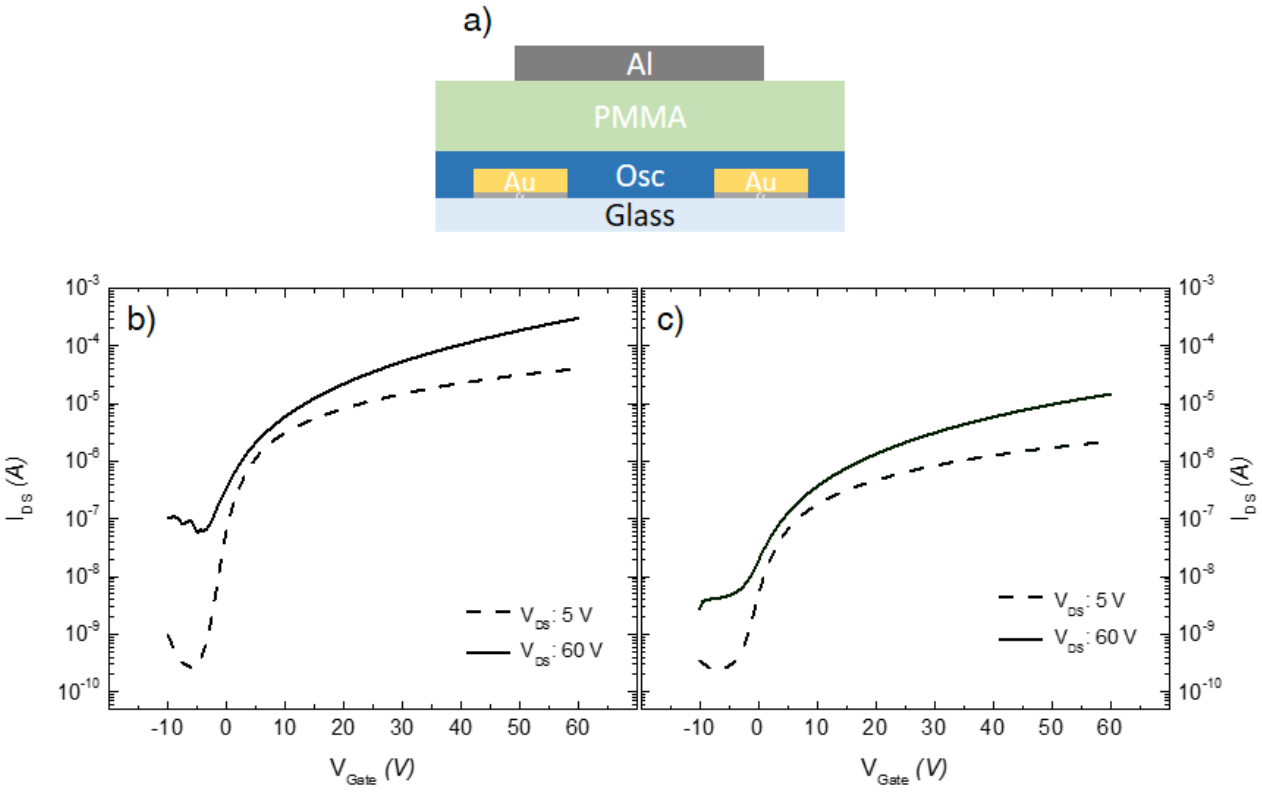

Figure S5. (a) Sketch of the top-gate, bottom-contacts geometry adopted for the fabrication of FET (channel length L = 20 µm and channel width W = 200 µm). Typical transfer characteristics of (b) PNDIT2 and (c) 2S-*trans*-PNDIT2

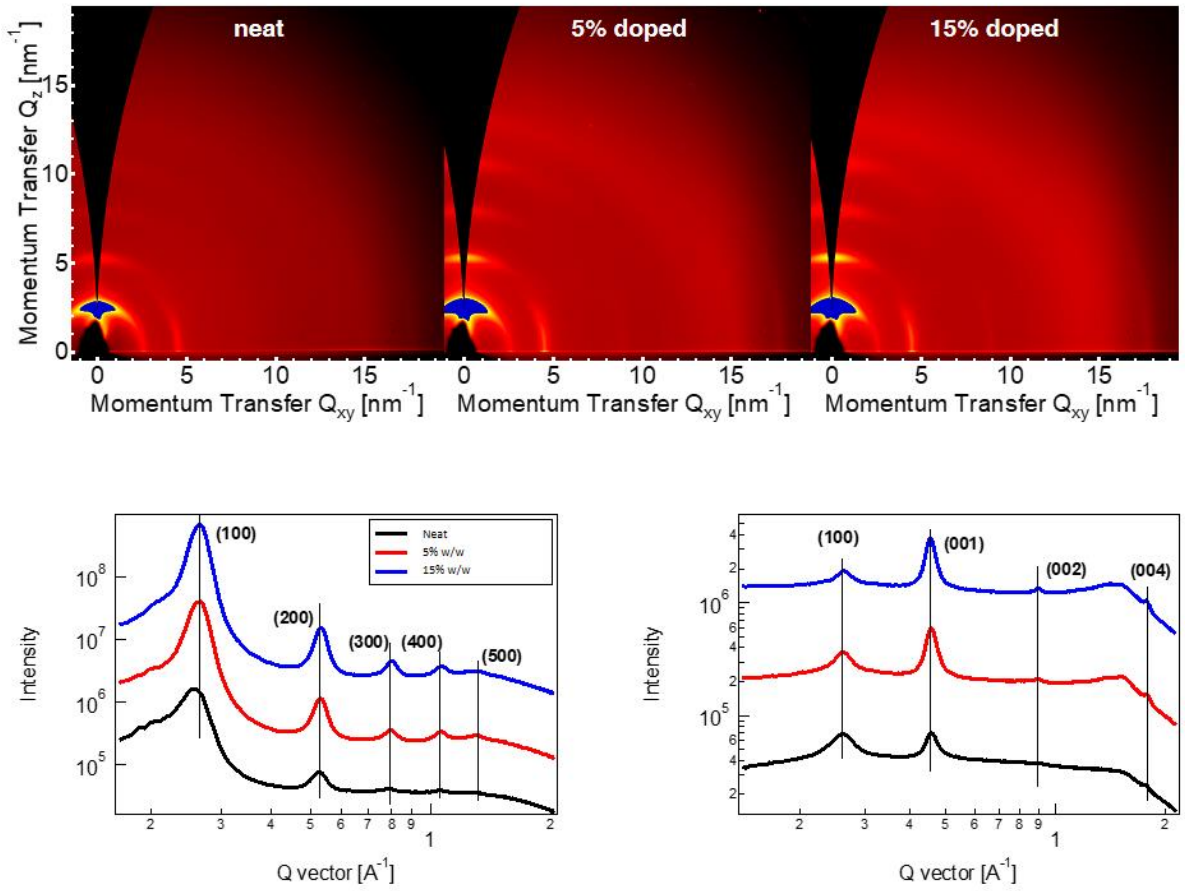

Figure S6. Two-dimensional GIWAXS patterns of PNDIT2 films for different doping concentrations, 0, 5, 15% w/w. Corresponding one-dimensional out-of-plane (bottom left) and in-plane (bottom right) GIWAXS profiles.

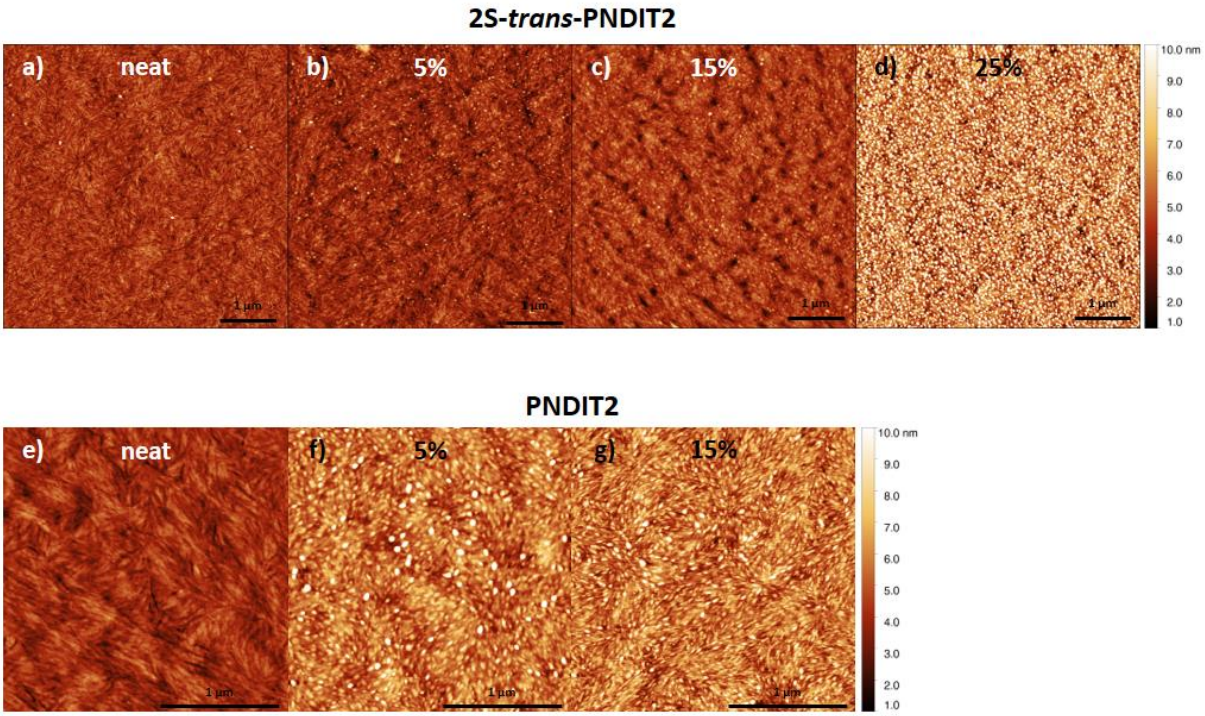

Figure S7. AFM images of 2S-*trans*-PNDIT2 films: (a) pristine, (b) 5 % w/w N-DPBI, (c) 15 % w/w N-DPBI, (d) 25 % w/w N-DPBI and PNDIT2 films (e) pristine, (f) 5 % w/w N-DPBI, (g) 15 % w/w N-DPBI.

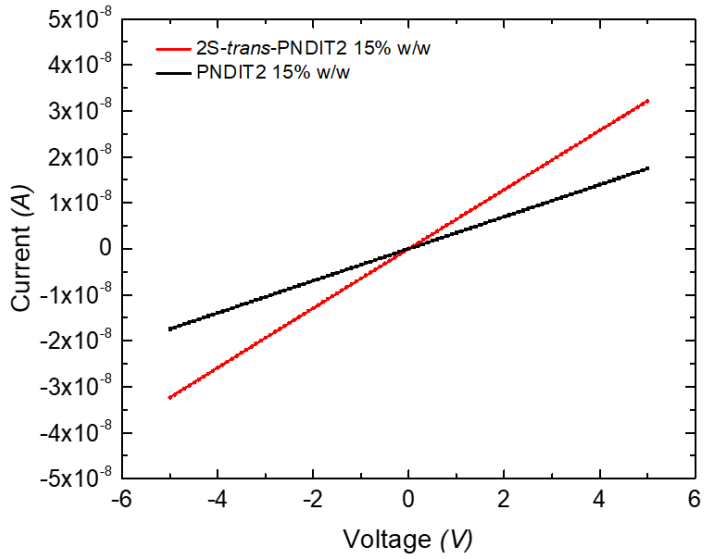

Figure S8. Current/Voltage curves for 2S-*trans*-PNDIT2 and PNDIT2 doped at 15 % w/w with N-DPBI reported as example. Electrical conductivities reported in Figure 2a and c were extracted from the slope of the Current/Voltage curves.

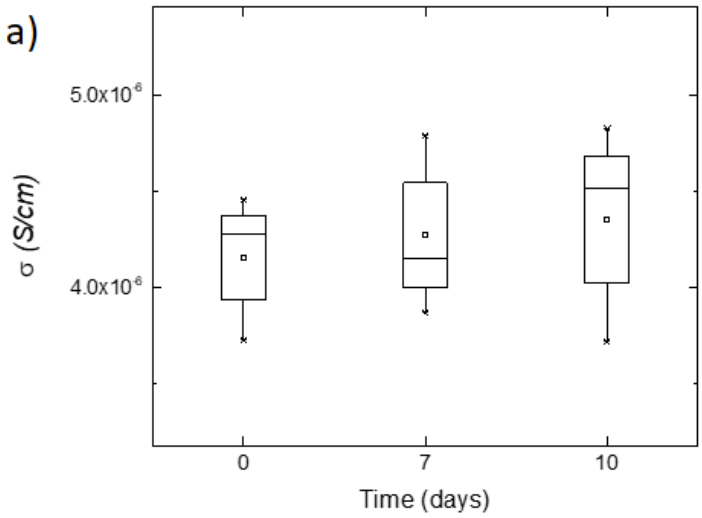
a)
5.0x10⁻⁶
4.0x10⁻⁶
σ (S/cm)
0
7
10
Time (days)

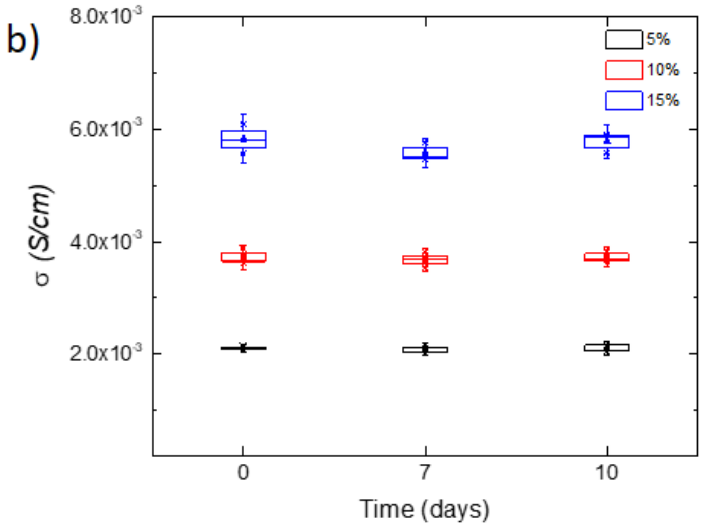
b)
8.0x10⁻³
6.0x10⁻³
4.0x10⁻³
2.0x10⁻³
σ (S/cm)
5%
10%
15%
0
7
10
Time (days)

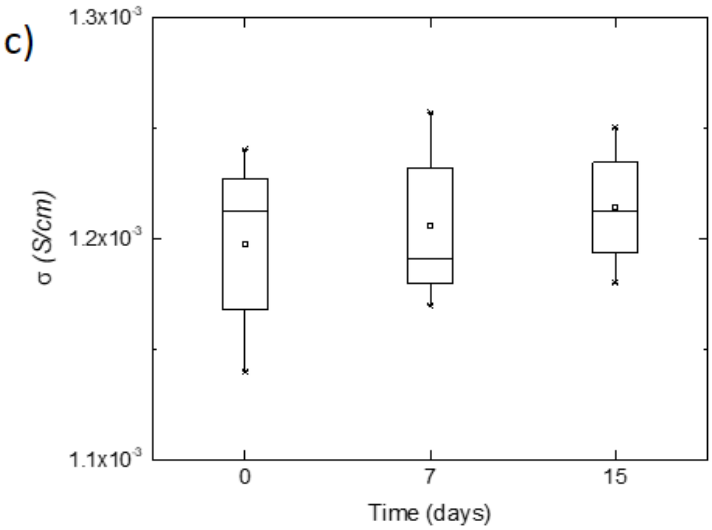
c)
1.3x10⁻³
1.2x10⁻³
1.1x10⁻³
σ (S/cm)
0
7
15
Time (days)

Figure S9. Time dependence of the electrical conductivity of non-encapsulated thin films of 2S-*trans*-PNDIT2 and PNDIT2 stored in inert ambient conditions (O_2 and H_2O concentration < 5ppm) at different N-DPBI concentrations: a) neat 2S-*trans*-PNDIT2, b) 5-15% w/w 2S-*trans*-PNDIT2 c) 15% w/w PNDIT2. Each data point is an average of at least four devices, box plots represent the standard deviation.

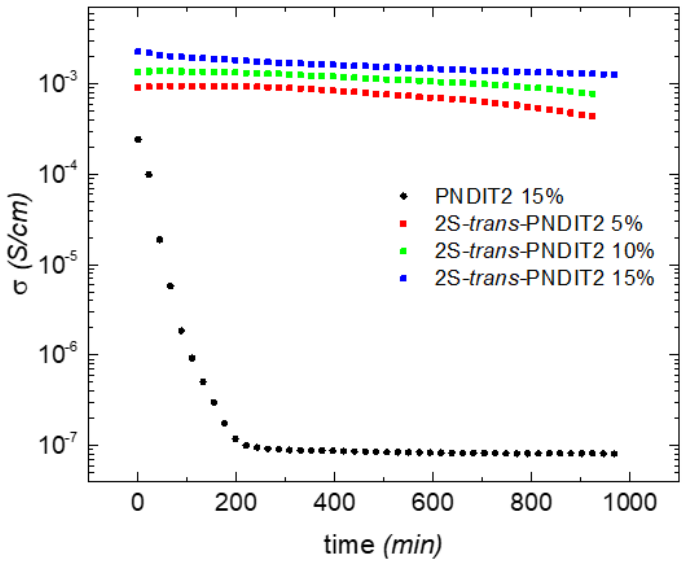

Figure S10 Time dependence of the electrical conductivity of non-encapsulated thin films of 2S-*trans*-PNDIT2 at different dopant concentrations (red 5% w/w, green 10% w/w and blue 15% w/w) and PNDIT2 (black dots), with 15 % w/w N-DPBI, upon ambient air exposure.

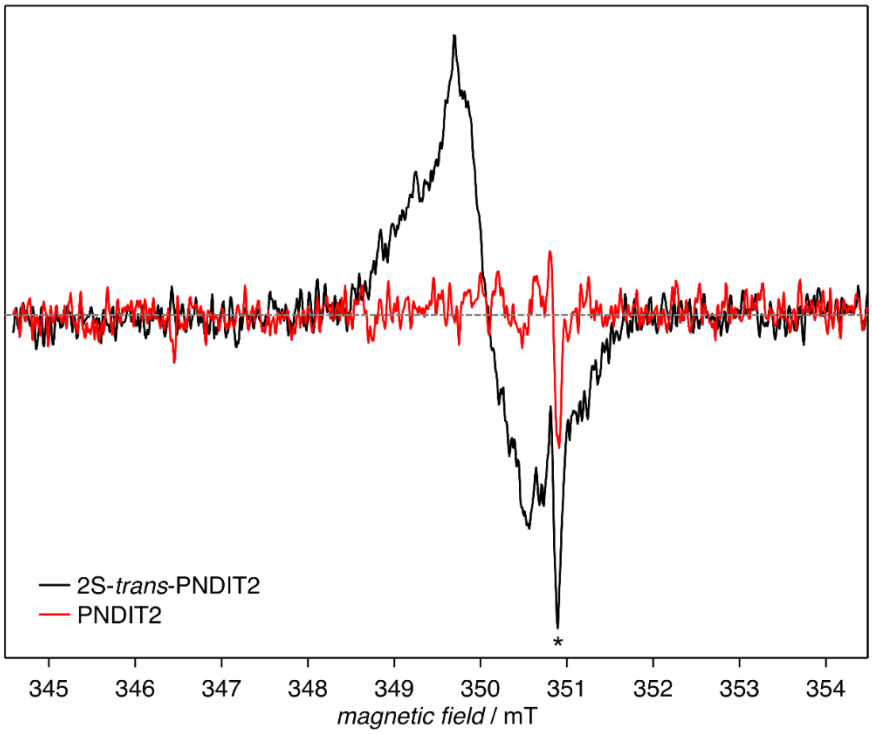

Figure S11: ESR spectra of undoped, neat 2S-*trans*-PNDIT2 and PNDIT2 films drop-cast on quartz-glass substrate. The sharp signal at about 351 mT marked with an asterisk is an artifact from the sample tube. As obvious from the spectra, only 2S-*trans*-PNDIT2 shows a weak ESR signal, whereas for PNDIT2, no ESR signal can be detected.

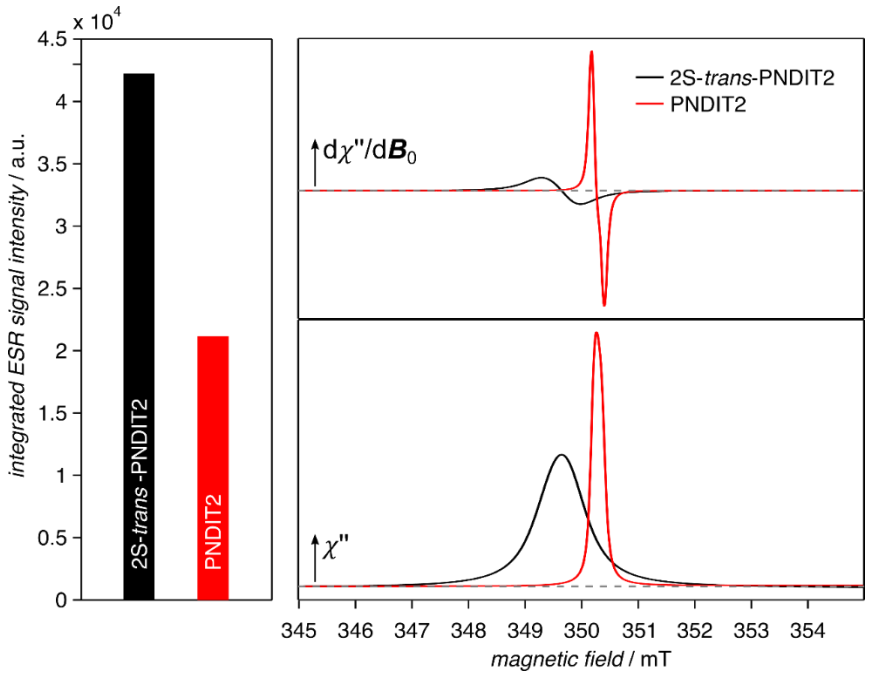

Figure S12: Quantitative comparison of ESR signals for 2S-*trans*-PNDIT2 and PNDIT2 films doped with N-DPBI (15% w/w) and annealed at 150 °C for 120 min. Field-modulated ESR signals shown in the top-right panel and appearing with first-derivative line-shape have been integrated (bottom right) and the area below the integrated spectra has been compared (bar graph to the left). As obvious from the direct comparison, 2S-*trans*-PNDIT2 shows about twice as strong an ESR signal as compared to PNDIT2, what directly translates into twice the charge carrier density in 2S-*trans*-PNDIT2. χ'' denotes the complex part of the magnetic susceptibility, hence the absorption of microwave by the sample.

References

(1) Shin, Y.; Welford, A.; Komber, H.; Matsidik, R.; Thurn-Albrecht, T.; McNeill, C. R.; Sommer, M. Regioregular Polymer Analogous Thionation of Naphthalene Diimide − Bithiophene Copolymers. *Macromolecules* **2018**, 51, 984-99.

(2) Luzio, A.; Fazzi, D.; Natali, D.; Giussani, E.; Baeg, K. J.; Chen, Z.; Noh, Y. Y.; Facchetti, A.; Caironi, M. Synthesis, Electronic Structure, and Charge Transport Characteristics of Naphthalenediimide-Based Co-Polymers with Different Oligothiophene Donor Units. *Adv. Funct. Mater.* **2014**, 24 1151–1162.

(3) Pommerehne, J.; Vestweber, H.; Guss, W.; Mahrt, R. F.; Bässler, H.; Porsch, M.; Daub, J. Efficient Two Layer Leds On A Polymer Blend Basis. *Adv. Mater.* **1995**, 7, 551.

(4) Berti, G.; Calloni, A.; Brambilla, A.; Bussetti, G.; Duò, L.; Ciccacci, F. Direct Observation Of Spin-Resolved Full And Empty Electron States. *Rev. Sci. Instrum.* **2014**, 85, 73901-73908.

(5) Vancea, J.; Reiss G.; Schneider, F.; Bauer, K.; Hoffmann, H.;Substrate Effects On The Surface Topograph,y Of Evaporated Gold Films: A Scanning Tunnelling Microscopy Investigation. *Surf. Sci.* **1989**, 218, 108-116.

(6) Moore, J.R; Albert-Seifried, S; Rao, A.; Massip, S.; Watts, B.; Morgan, D.J.; Friend, R.H.; McNeill, C.R;, Sirringhaus, H. Polymer Blend Solar Cells Based on a High-Mobility Naphthalenediimide-Based Polymer Acceptor: Device Physics, Photophysics and Morphology. *Adv. Energy Mater*. **2011**, 1, 230.

(7) Onoufriou, D.; Yim, S.; Jone,s T.S. Me-PTCDI Thin Film Deposition On Insb(1 1 1). *Surf. Sci.* **2004**, 573, 237.

(8) Brambilla, A.; Calloni, A.; Aluicio-Sardui, E.; Berti, G.; Kan, Z.; Beaupré, S.; Leclerc, M.; Butt, H.-J.; Floudas, G.; Keivanidis, P. E. X-Ray Photoemission Spectroscopy Study of Vertical PhaseSeparation in F8BT:PDI/ITO Films for Photovoltaic Applications. In SPIE NanoScience +Engineering; Banerji, N.; Hayes, S. C.; Silva, C., Eds.; International Society for Optics and Photonics, **2014**; pp. 91650C/1–91650C/9.

(9) Fratesi, G.; Lanzilotto ,V.; Stranges, S.; Alagia, M.; Brivio, G.P.; Floreano, L. High Resolution NEXAFS Of Perylene And PTCDI: A Surface Science Approach To Molecular Orbital Analysis *Phys. Chem. Chem. Phys*. **2014**, 16, 14834.

(10) Schöll, A.; Zou Y.; Jung, M.; Schmidt, T.; Fink, R.; Umbach, E. Line Shapes and Satellites In High-Resolution X-Ray Photoelectron Spectra Of Large Pi-Conjugated Organic Molecules. *J. Chem. Phys.* **2004**, 121, 10260.

(11) Edwards, D.A.; Richards, R.; Myers, R.E.; Walton, R.A. Isoperthiocyanic Acid (3-Amino-5-Thione-L,2,4-Dithiazole): An Exocyclic Sulphur Donor Ligand *Inorganica Chim. Acta* **1977,** 23, 215.

(12) Calloni, A.; Brambilla, A.; Berti, G.; Bussetti, G.; Canesi, E. V.; Binda, M.; Petrozza, A.; Finazzi, M.; Ciccacci, F.; Duò, L. X-Ray Photoemission Spectroscopy Investigation Of The Interaction Between 4-Mercaptopyridine And The Anatase TiO_2 Surface. *Langmuir*, **2013**, 29, 8302-8309.

(13) Aluicio-Sarduy, E.; Singh, R.; Kan, Z.; Ye, T.; Baidak, A.; Calloni, A.; Berti, G.; Duò, L.; Iosifidis, A.; Beaupré, S.; Leclerc, M.; Butt, H.-J.; Floudas, G.; Keivanidis, P. E. Elucidating the Impact of Molecular Packing and Device Architecture on the Performance of Nanostructured Perylene Diimide Solar Cells *ACS Appl. Mater. Interfaces* **2015**, 7, 8687–8698

(14) Shi, K.; Zhang, F.; Di, C.A.; Yan, T.W.; Zou, Y.; Zhou, X.; Zhu, D.; Wang, J.W.; Pei, J. Toward High Performance n-Type Thermoelectric Materials by Rational Modification of BDPPV Backbones *J. Am. Chem. Soc.* **2015**, 137, 6979-6989

(15) Naab, B. D.; Guo, S.; Olthof, S.; Evans, E. G. B.; Wei, P.; Millhauser, G. L.; Kahn, A.; Barlow, S.; Marder, S. R.; Bao, Z. Mechanistic Study on the Solution-Phase N-Doping of 1,3-Dimethyl- 2-Aryl-2,3-Dihydro-1H-benzoimidazole Derivatives. *J. Am. Chem. Soc.* **2013**, *135*, 15018–15025.